Entangling optical and mechanical cavity modes in an optomechanical crystal nanobeam

Qizhi Cai,[1] Boyu Fan,[1,*] Yunru Fan,[1] Guangwei Deng,[1] You Wang,[1,2] Haizhi Song,[1,2] Guangcan Guo,[1,3] and Qiang Zhou[1,3,†]

[1]*Institute of Fundamental and Frontier Sciences, University of Electronic Science and Technology of China, Chengdu, Sichuan, People's Republic of China*

[2]*Southwest Institute of Technical Physics, Chengdu, Sichuan, People's Republic of China*

[3]*CAS Key Laboratory of Quantum Information, University of Science and Technology of China, Hefei, People's Republic of China*

(Received 11 April 2023; revised 6 July 2023; accepted 11 July 2023; published 23 August 2023)

A scheme for the generation of steady-state entanglement between optical and mechanical cavity modes in an optomechanical crystal nanobeam is proposed. Based on finite element simulation and the quantum Langevin equation, we explore the evolution of entanglement with optomechanical properties in various device configurations, and demonstrate the ability of optimal entanglement generation in both blue and red detuned optical pumps. The intrinsic relationship between optomechanical cooperativity and entanglement is further clarified for depicting a clear physical picture of optomechanical interaction. Our work expands the understanding of macroscopic quantum mechanics and is an important step for developing novel quantum optomechanical devices.

DOI: 10.1103/PhysRevA.108.022419

I. INTRODUCTION

The spooky phenomenon of quantum entanglement not only enhances our understanding of the physical world, but also presents new opportunities for innovation and advancement in information science and technology [1]. In recent decades, numerous studies have reported on entanglement generation using different physical platforms and information carriers [2–14], wherein optomechanical systems have emerged as particularly promising platforms due to their versatility in design, fabrication, and control [15,16]. In optomechanical systems, momentum is exchanged between mechanical objects and electromagnetic radiation, providing one pathway towards bipartite and multipartite entanglement between phonons, optical and microwave photons, such as microwave radiation and mechanical modes [17], two microwave radiations [18], two optical modes [19], and two mechanical modes [20]. Among various designs of optomechanical systems, the optomechanical crystal nanobeam shows merits of high sensitivity, tunability, and compactness, making related research prosperous in recent years—for instance, realization of entanglement between two mechanical oscillators with the medium of light [8], transduction between microwave and optical signals [21,22], mechanical quantum memory controlled through optical interface [23], demonstration of violating Bell inequality [24], and quantum teleportation [25] involving massive and macroscopic optomechanical crystals. However, the steady-state entanglement between optical and mechanical cavity modes in nanobeam structure remains elusive, which may hinder the development of multipartite entanglement and applications mentioned above based on the nanobeam platforms.

In this work, we propose a theoretical scheme to generate steady-state entanglement between optical and mechanical modes in a single optomechanical crystal nanobeam. By conducting finite element simulations, the effects of structural parameters on device properties, i.e., single-photon coupling rate, mechanical and optical resonant frequencies, and quality factors that primarily determine the entanglement, are analyzed. We model the dynamics using the standard Langevin formalism and quantify the entanglement at steady state via logarithmic negativity, thereafter the optimal parameter regimes in blue and red detuned optical pumps are comprehensively presented. Comparing the performance between cooperativity and entanglement, optomechanical interaction pictures are depicted. Our results are expected to be applied in the device design for microwave-optical quantum transducers and optical information processing.

II. MODEL

As shown in Fig. 1(a), we consider a single optomechanical crystal cavity, including an integrated optical and mechanical nanoscale resonator within two mirror regions, formed in the surface layer of a silicon-on-insulator microchip. In principle, the pump light with angular frequency ω_{do} can pump into the cavity and resonate at ω_o, then the mechanical modes are driven via radiation pressure, building the optomechanical interaction shown in Fig. 1(d). The total Hamiltonian of the considered system reads [26]

$$H_0 = \hbar\omega_o \hat{a}^\dagger \hat{a} + \frac{\hbar\omega_m}{2}(\hat{p}^2 + \hat{q}^2) - \hbar G_0 \hat{a}^\dagger \hat{a}\hat{q} + i\hbar E(e^{-i\omega_{do}t}\hat{a}^\dagger - e^{i\omega_{do}t}\hat{a}), \quad (1)$$

where $\hat{q}$ and $\hat{p}$ are the dimensionless position and momentum quadratures of the mechanical mode, satisfying $[\hat{q}, \hat{p}] = i$. $\hat{a}$ and $\hat{a}^\dagger$ ($[\hat{a}, \hat{a}^\dagger] = 1$) are the annihilation and creation operator

*fby@uestc.edu.cn
†zhouqiang@uestc.edu.cn

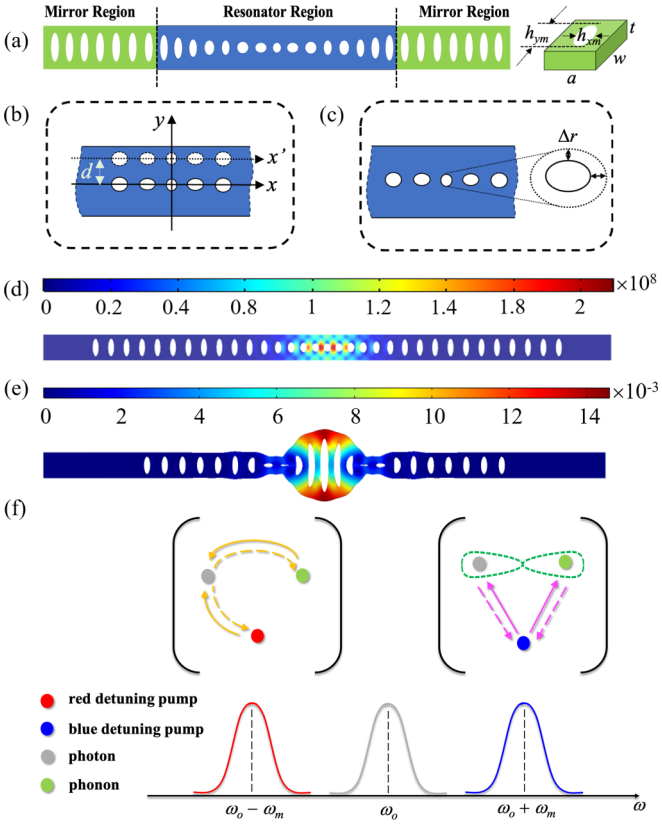

FIG. 1. (a) Plane-view schematic diagram of the silicon optomechanical crystal nanobeam cavity and unit cell geometry in the mirror region, where h_{xm} and h_{ym} correspond to the width and length of the hole in the optomechanical crystal, and a, w, and t are the length, width, and height of the hole unit. (b and c) Schematic representation of hole's position d and unitary variation of hole dimension Δr in nanobeam cavity. (d) E_y component of optical fundamental mode at telecom band. (e) Displacement field of the corresponding fundamental breathing mode. (f) Photon-phonon interaction picture with red and blue detuned pump. Red detuned pump results in an interaction reminiscent of a beam splitter, where a pump photon absorbs a phonon to generate a resonant photon and vice versa. Blue detuned pump results in an interaction of parametric down-conversion type, in which a pump photon converts to a resonant photon and a phonon.

of the cavity modes. G_0 is the single-photon coupling rate between the optical and mechanical modes, which is calculated via device simulation in this work, and E is related to the pump optical power P and decay rate $\kappa = \omega_o/Q_o$ (Q_o is the optical quality factor) by $|E| = \sqrt{2P\kappa/\hbar\omega_{do}}$.

By considering the damping and the corresponding Brownian noise of both optical and mechanical modes, the nonlinear quantum Langevin equations (QLEs) written in the interaction picture with respect to $\hbar\omega_{do}\hat{a}^\dagger\hat{a}$ are

$$\begin{aligned}\dot{\hat{q}} &= \omega_m\hat{p},\\ \dot{\hat{p}} &= -\omega_m\hat{q} - \gamma_m\hat{p} + G_0\hat{a}^\dagger\hat{a} + \xi,\\ \dot{\hat{a}} &= (i\Delta_0 - \kappa)\hat{a} + iG_0\hat{a}\hat{q} + E + \sqrt{2\kappa}\hat{a}^{in},\end{aligned} \tag{2}$$

where $\Delta_0 = \omega_{do} - \omega_o$ and $\gamma = \omega_m/Q_m$ is the mechanical damping rate with mechanical quality factor Q_m. The zero-mean vacuum radiation input noise a^{in} satisfies correlation functions [27]

$$\begin{aligned}\langle a^{in}(t)a^{in,\dagger}(t')\rangle &= \delta(t-t'),\\ \langle a^{in,\dagger}(t)a^{in}(t')\rangle &= 0,\end{aligned} \tag{3}$$

and the Hermitian Brownian noise operator ξ has the correlation function [27]

$$\langle\xi(t)\xi(t')\rangle = \frac{\gamma_m}{\omega_m}\int\frac{d\omega}{2\pi}e^{-i\omega(t-t')}\omega\left[\coth\left(\frac{\hbar\omega}{2k_BT}\right)+1\right], \tag{4}$$

in which k_B is the Boltzmann constant and T is the environment temperature. In the limit of high mechanical quality factor $Q_m \gg 1$, $\xi(t)$ could be considered as Markovian, whose correlation function is reduced to $\langle\xi(t)\xi(t') + \xi(t')\xi(t)\rangle/2 \approx \gamma_m(2\bar{n}_m + 1)\delta(t-t')$ [28], where $\bar{n}_m = 1/[\exp(\hbar\omega_m/k_BT) - 1]$ is the mean thermal excitation number of the mechanical modes.

One could always rewrite each mode operator as the sum of a constant steady number and an additional fluctuation operator with zero-mean value, namely, $\hat{a} = \alpha_s + \delta\hat{a}$, $\hat{p} = p_s + \delta\hat{p}$, and $\hat{q} = q_s + \delta\hat{q}$. Let all derivatives in QLEs be zero, the steady-state mean values of the optical and mechanical modes are presented as follows:

$$\begin{aligned}p_s &= 0,\\ q_s &= \frac{G_0|\alpha_s|^2}{\omega_m},\\ \alpha_s &= \frac{E}{\kappa - i\Delta},\end{aligned} \tag{5}$$

where $\Delta = \Delta_0 + G_0q_s$ is the effective optical detuning. We assume that the optical mode is strongly driven, i.e., $|\alpha_s| \gg 1$, then one could safely neglect the nonlinear terms and obtain the linearized Langevin equations

$$\begin{aligned}\delta\dot{\hat{q}} &= \omega_m\delta\hat{p},\\ \delta\dot{\hat{p}} &= -\omega_m\delta\hat{q} - \gamma_m\delta\hat{p} + G\delta\hat{X} + \xi,\\ \delta\dot{\hat{X}} &= -\kappa\delta\hat{X} - \Delta\delta\hat{Y} + \sqrt{2\kappa}\hat{X}^{in},\\ \delta\dot{\hat{Y}} &= -\kappa\delta\hat{Y} + \Delta\delta\hat{X} + G\delta\hat{q} + \sqrt{2\kappa}\hat{Y}^{in},\end{aligned} \tag{6}$$

where we have chosen the appropriate phase reference of the optical cavity field so that α_s could be taken as real and positive. The cavity field quadratures are defined as $\delta\hat{X} = (\delta\hat{a} + \delta\hat{a}^\dagger)/\sqrt{2}$ and $\delta\hat{Y} = (\delta\hat{a} - \delta\hat{a}^\dagger)/i\sqrt{2}$, the corresponding input noise terms are $\hat{X}^{in} = (\hat{a}^{in} + \hat{a}^{in,\dagger})/\sqrt{2}$ and $\hat{Y}^{in} = (\hat{a}^{in} - \hat{a}^{in,\dagger})/i\sqrt{2}$, and the effective optomechanical coupling $G = G_0\alpha_s\sqrt{2}$.

Since the noise operators ξ and $\hat{a}_{in}$ are zero-mean Gaussian and the dynamics is linearized now, the quantum steady state of the system is fully characterized by a 4×4 covariance matrix with its elements $V_{ij} = \langle u_i(\infty)u_j(\infty) + u_j(\infty)u_i(\infty)\rangle/2$, where $u^T(\infty) = [\delta\hat{q}(\infty), \delta\hat{p}(\infty), \delta\hat{X}(\infty), \delta\hat{Y}(\infty)]$ represents the steady-state fluctuation operators. Thereafter, Eq. (6) could be rewritten as a matrix form

$$\dot{u}(t) = Au(t) + n(t), \tag{7}$$

where $n^T(t) = [0, \xi(t), \sqrt{2\kappa}\hat{X}^{in}(t), \sqrt{2\kappa}\hat{Y}^{in}(t)]$ and matrix

$$A = \begin{pmatrix} 0 & \omega_m & 0 & 0 \\ -\omega_m & -\gamma_m & G & 0 \\ 0 & 0 & -\kappa & -\Delta \\ G & 0 & \Delta & -\kappa \end{pmatrix}. \tag{8}$$

The solution of Eq. (7) is

$$u(t) = M(t)u(0) + \int_0^t dsM(s)n(t-s), \tag{9}$$

with $M(t) = e^{At}$. The system is stable when $M(\infty) = 0$ that is equivalent to all eigenvalues of A have negative real parts, which could be derived by Routh-Hurwitz criterion [26]. Without special statements, the parameter regime used satisfies the Routh-Hurwitz criterion in the following numerical simulation.

When the system is stable, the elements of the covariance matrix read

$$V_{ij} = \sum_{k,l} \int_0^\infty ds \int_0^\infty ds' M_{ik}(s) M_{jl}(s') \Phi_{kl}(s-s'), \tag{10}$$

where $\Phi_{kl}(s-s') = \langle n_k(s) n_l(s') + n_l(s') n_k(s) \rangle / 2$ is the matrix of stationary noise correlation functions. One could also write $\Phi_{kl}(s-s') = D_{kl}\delta(s-s')$, where $D_{kl} = \mathrm{Diag}[0, \gamma_m(2\bar{n}_m + 1), \kappa, \kappa]$. Then Eq. (10) becomes

$$V = \int_0^\infty dsM(s)DM^T(s). \tag{11}$$

With $M(\infty) = 0$ and Lyapunov's first theorem, Eq. (11) is equivalent to

$$AV + VA^T = -D. \tag{12}$$

By solving Eq. (12), matrix $V = \begin{pmatrix} V_1 & V_3 \\ V_3^T & V_2 \end{pmatrix}$ that describes the optomechanical system could be obtained. Then, logarithmic negativity that quantifies the steady-state optomechanical entanglement is [29,30]

$$E_n = \max[0, -\ln 2\eta^-], \tag{13}$$

where $\eta^- \equiv \sqrt{\Sigma V - \sqrt{(\Sigma V)^2 - 4 \det V}}/\sqrt{2}$ and $\Sigma V \equiv \det V_1 + \det V_2 - 2 \det V_3$.

III. RESULTS

In Fig. 2, we modulate Q_o and Q_m over a wide range while minimizing the fluctuation of ω_o, ω_m, and G_0 by changing h_{xm} in the mirror region [31–34]. The entanglement with effective detuning $\Delta = -\omega_m$ and $\Delta = 0.8\omega_m$ is presented. Due to the Routh-Hurwitz criterion, $\Delta = 0.8\omega_m$ is chosen instead of $\Delta = \omega_m$, with ignoring this limitation in the pulsed operation case [35,36]. We could find that the entanglement at $\Delta = -\omega_m$ gains its maximum value at $h_{xm} = 130$ nm, while the $\Delta = 0.8\omega_m$ situation obtains its comparatively large value at $h_{xm} = 250$ nm and 260 nm. For each point, the error bars in entanglement dots are the standard deviation with ±10% fluctuations of input optical power. In the following results, we fix $h_{xm} = 130$ nm for analyzing the entanglement properties

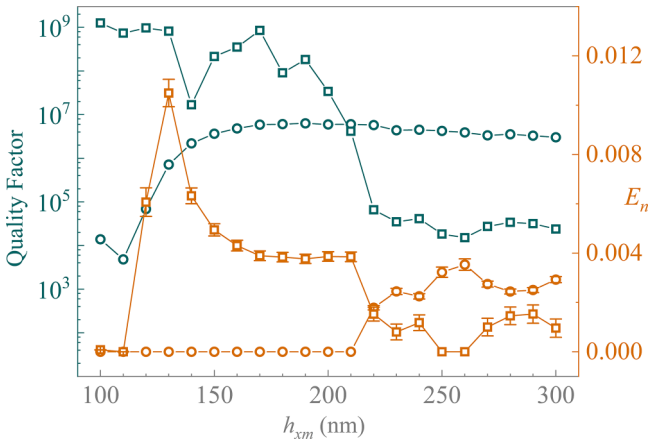

FIG. 2. Optical quality factor Q_o (green circle), mechanical quality factor Q_m (green square), and entanglement with two effective detuning $\Delta = -\omega_m$ (orange dot) and $\Delta = 0.8\omega_m$ (orange square) versus h_{xm}. The hole's position d and unitary variation of hole dimension Δr are equal to zero. The error bars in entanglement dots are the standard deviation with ±10% fluctuations of input optical power. The temperature $T = 10$ mK and optical pump $P = 10$ mW, where $\omega_o \approx 2\pi \times 192.6$ THz, $\omega_m \approx 2\pi \times 5.17$ GHz, and $G_0 \approx 1.03 \times 10^6$ are nearly unchanged.

in the red detuned case and both $h_{xm} = 250$ nm and 260 nm in the blue detuned case.

In the case of red detuned driving $\Delta = -\omega_m$, the trend of entanglement and cooperativity defined by $\Gamma = G^2/\kappa\gamma_m$ is basically consistent as shown in Figs. 3(a)–3(d). In fact, optical and mechanical excitations are effectively exchanged, where high cooperativity corresponds to larger entanglement. Note that E_n as well as Q_o monotonically increases as Δr range from −10 nm to −4 nm. In this region, Q_o is comparatively small on the order of $10^5 \sim 10^6$, resulting in large optical damping. The few intracavity photons contribute to a tiny amount of E_n. Furthermore, the entanglement versus both d and Δr is shown in Fig. 3(e), where the light gray area corresponds to the unstable parameter regime in which $E_n = 0$. Entanglement larger than 10^{-2} can be realized within a certain range, which provides valuable guidance for device design improvement. In Fig. 3(f), as the temperature is increased to 1 K, we observe a monotonic decrease in entanglement due to quantum decoherence between the interaction modes. In contrast, entanglement is found to be proportional to the optical power pump owing to enhanced cavity photons.

With blue detuning, $\Delta = 0.8\omega_m$, one could find that the cooperativity nearly possesses the same trend with Q_m in the parameter regime of our simulation, and the entanglement behaves oppositely compared with cooperativity, where Refs. [37,38] had found a similar behavior. In Fig. 4(e), E_n versus d and Δr is analyzed, and the parameter range where entanglement is maximized is limited compared to Fig. 3(e), calling for more stringent requirements for fabrication precision. Figure 4(f) chooses the maximum entanglement point to analyze the influence of temperature and optical pump on the entanglement, obtaining the same law as Fig. 3(f). In the case of $h_{xm} = 260$ nm, despite the maximum entanglement being slightly improved as shown in Fig. 5, the drastic deterioration

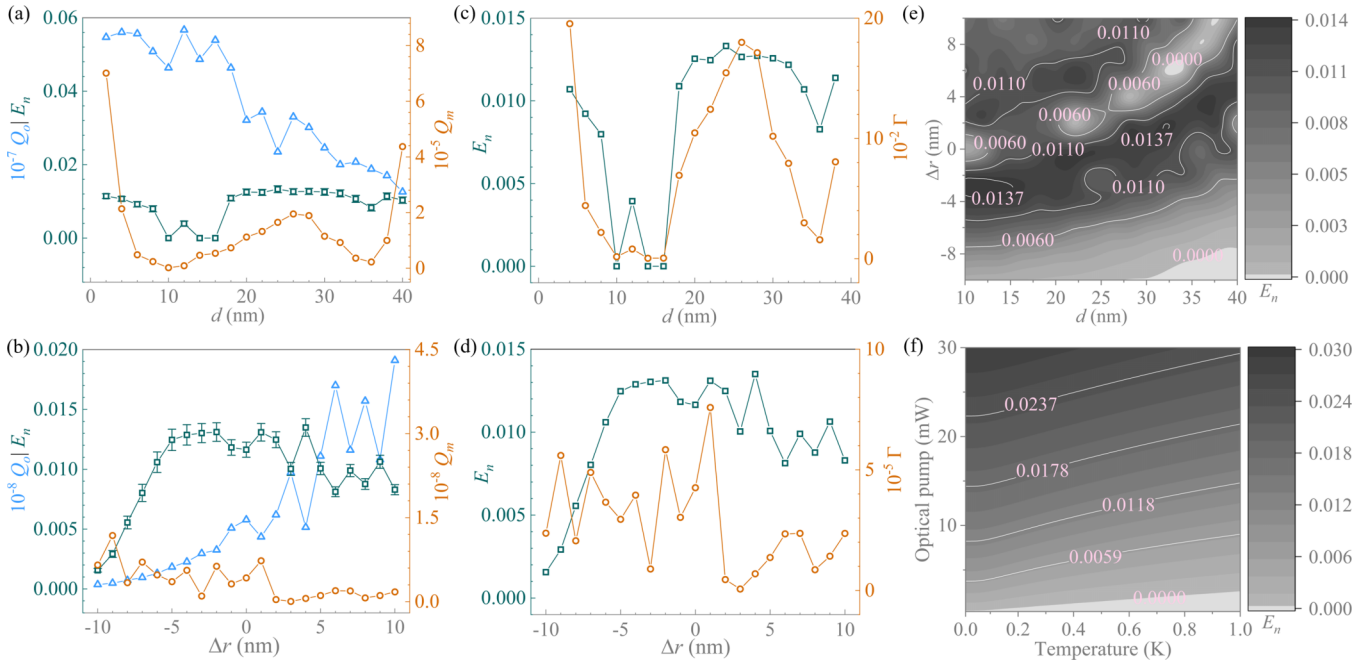

FIG. 3. The entanglement properties with red detuning $\Delta = -\omega_m$. (a and b) Q_o (blue triangle) and Q_m (orange circle) versus d and Δr and entanglement (green square). The error bars are the standard deviation of $\pm 10\%$ fluctuations in input optical power. (c and d) Entanglement (green square) and cooperativity (orange circle) versus d and Δr. (e) Entanglement versus both d and Δr. (f) For maximum entanglement point in (e), the parameters are optical angular resonant frequency $\omega_o = 2\pi \times 1.94 \times 10^{14}$ Hz, mechanical angular resonant frequency $\omega_m = 2\pi \times 5.17 \times 10^9$ Hz, optical quality factor $Q_o = 2.17 \times 10^5$, mechanical quality factor $Q_m = 8.59 \times 10^4$, and single-photon coupling rate $G_0 = 1.07 \times 10^6$, the temperature range is 0∼1 K and optical pump ranges from 0 to 30 mW. Other parameters: $h_{xm} = 130$ nm, temperature $T = 10$ mK, and optical pump $P = 10$ mW in (a)–(e).

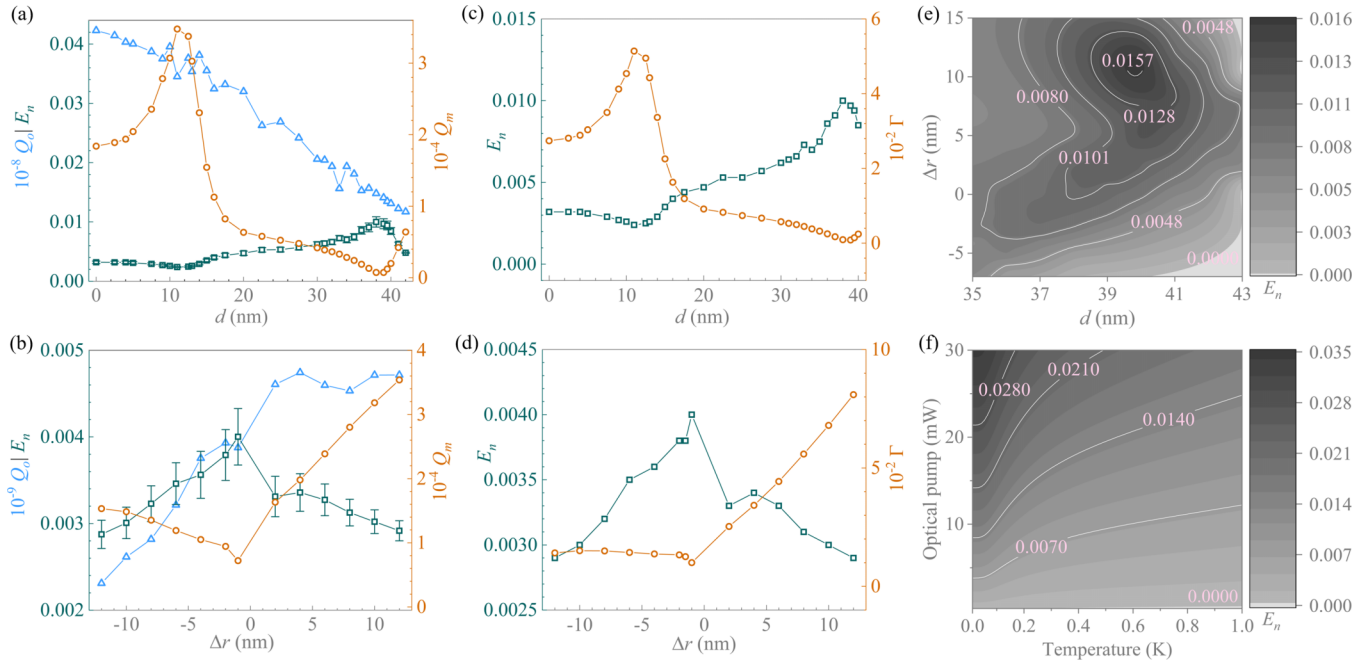

FIG. 4. Entanglement properties with blue detuning $\Delta = 0.8\omega_m$. (a and b) Q_o (blue triangle) and Q_m (orange circle) versus d and Δr and entanglement (green square). The error bars are the standard deviation of $\pm 10\%$ fluctuations in input optical power. (c and d) Entanglement (green square) and cooperativity (orange circle) versus d and Δr. (e) Entanglement versus both d and Δr. (f) For the maximum entanglement point in (c), the parameters are optical angular resonant frequency $\omega_o = 2\pi \times 1.98 \times 10^{14}$ Hz, mechanical angular resonant frequency $\omega_m = 2\pi \times 4.92 \times 10^9$ Hz, optical quality factor $Q_o = 1.30 \times 10^6$, mechanical quality factor $Q_m = 5.66 \times 10^2$, and single-photon coupling rate $G_0 = 1.06 \times 10^6$, the temperature range is 0∼1 K, and optical pump ranges from 0 to 30 mW. Other parameters: $h_{xm} = 250$ nm, temperature $T = 10$ mK, and optical pump $P = 10$ mW in (a)–(e).

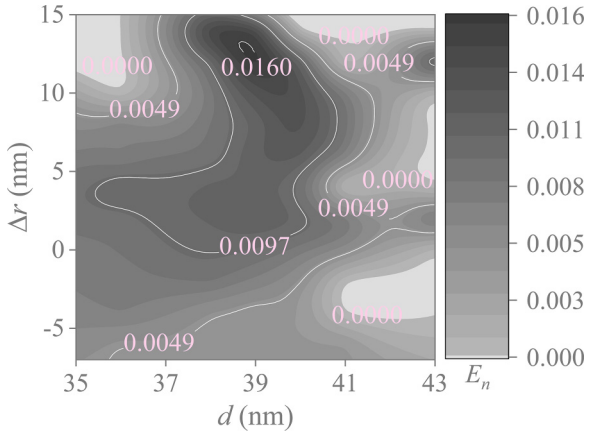

FIG. 5. The entanglement properties with blue detuning $\Delta = 0.8\omega_m$ versus both d and Δr for $h_{xm} = 260$ nm, in which temperature $T = 10$ mK and optical pump $P = 10$ mW.

of the stability region is also observed. A comprehensive consideration should be moved toward detailed device design.

We also calculate the entanglement rates E_r, which are given by $E_r = E_f B$ [18,39,40]. The entropy of formation $E_f = \sigma_+ \log_2 \sigma_+ - \sigma_- \log_2 \sigma_-$, where $\sigma_\pm = (1/\sqrt{\theta} \pm \sqrt{\theta})^2/4$ with $\theta = 2^{-E_n}$. The bandwidth of emitted radiation $B = (1 + \Gamma)\gamma_m$. For the maximum entanglement parameter regime in the red detuned case as shown in Fig. 3(f), the entanglement rates $E_r \approx 0.13$ Mebits/s, and the blue detuned counterpart $E_r \approx 0.33$ Mebits/s with parameters in Fig. 4(f). Compared to other generalized optomechanical systems [41,42], our scheme obtains the same order of magnitude.

In this section, we analyze the influence of the parameters decided by structural design on entanglement, i.e., ω_o, ω_m, Q_o, Q_m, and G_0, together with the environmental parameters T and P. Accompanied by explaining the standard theory of optomechanical entanglement, logarithmic negativity with its maximum 0.014 and 0.016 can be obtained in the region of detuning $\Delta = -\omega_m$ and $\Delta = 0.8\omega_m$. Moreover, the corresponding entanglement rates are calculated, reaching the same order compared with other similar systems. Our work is expected to expand the understanding of entanglement generation for the development of integrated entanglement sources based on optomechanical systems.

IV. CONCLUSION

We conduct a theoretical study of steady-state optomechanical entanglement in nanobeam structure, an area of research that has not been explored previously. Using finite element simulations and logarithmic negativity as the entanglement measure, we identify optimized parameter regimes in red and blue detuned optical pump situations. Our results show that the entanglement could reach an order of 10^{-2} and is robust against temperature. These findings provide guidance for the design of nanobeam structures for different application scenarios, as previously reported in literature [43–45]. For example, electrodes can be added at the end of phononic waveguides in nanobeam structures where microwave-to-light conversion is constructed through their common interaction with mechanical modes. In this case, the mechanical quality factor is inevitably attenuated to the order of 10^3. Our results indicate that the optomechanical entanglement could be generated with this parameter regime, providing a reference for further microwave-optical entanglement device design in this scheme. For optical information processing, our results can be applied to the entanglement generation between two optical modes of different frequencies in a nanobeam. The blue detuned optical mode could get entangled with the red detuned optical mode under proper parameter regimes. Our work covers the case of red detuning and blue detuning, which has instructive implications for the entanglement of two optical modes in nanobeams. Notably, the present electron beam lithography technique allows for fabrication accuracy of less than 1 nm [46], making it possible to develop practical devices in the future.

ACKNOWLEDGMENTS

This work was supported by the National Key Research and Development Program of China (Grants No. 2018YFA0307400 and No. 2018YFA0306102), the Sichuan Science and Technology Program (Grants No. 2021YFSY0063, No. 2021YFSY0062, No. 2021YFSY0064, No. 2021YFSY0065, No. 2021YFSY0066, No. 2022YFSY0061, No. 2022YFSY0062, and No. 2022YFSY0063), the National Natural Science Foundation of China (Grants No. U19A2076 and No. 62005039), and the Innovation Program for Quantum Science and Technology (Grant No. 2021ZD0301702).

Q.C. and B.F. contributed equally to this work.

[1] R. Horodecki, P. Horodecki, M. Horodecki, and K. Horodecki, Rev. Mod. Phys. **81**, 865 (2009).

[2] X. Liu, J. Hu, Z.-F. Li, X. Li, P.-Y. Li, P.-J. Liang, Z.-Q. Zhou, C.-F. Li, and G.-C. Guo, Nature (London) **594**, 41 (2021).

[3] D. Lago-Rivera, S. Grandi, J. Rakonjac, A. Seri, and H. de Riedmatten, Nature (London) **594**, 37 (2021).

[4] Y. Zhong, H. Chang, A. Bienfait, É. Dumur, M.-H. Chou, C. R. Conner, J. Grebel, R. G. Povey, H. Yan, D. I. Schuster *et al.*, Nature (London) **590**, 571 (2021).

[5] J. Yin, J.-G. Ren, H. Lu, Y. Cao, H.-L. Yong, Y.-P. Wu, C. Liu, S.-K. Liao, F. Zhou, Y. Jiang *et al.*, Nature (London) **488**, 185 (2012).

[6] E. Togan, Y. Chu, A. Trifonov, L. Jiang, J. Maze, L. Childress, M. V. G. Dutt, A. S. Sørensen, P. R. Hemmer, A. S. Zibrov *et al.*, Nature (London) **466**, 730 (2010).

[7] Y. Lin, D. R. Leibrandt, D. Leibfried, and C. Chou, Nature (London) **581**, 273 (2020).

[8] R. Riedinger, A. Wallucks, I. Marinković, C. Löschnauer, M. Aspelmeyer, S. Hong, and S. Gröblacher, Nature (London) **556**, 473 (2018).

[9] Y. Yu, F.Ma, X.-Y. Luo, B. Jing, P.-F. Sun, R.-Z. Fang, C.-W. Yang, H. Liu, M.-Y. Zheng, X.-P. Xie *et al.*, Nature (London) **578**, 240 (2020).

[10] P. C. Humphreys, N. Kalb, J. Morits, R. N. Schouten, R. F. L. Vermeulen, D. J. Twitchen, M. Markham, and R. Hanson, Nature (London) **558**, 268 (2018).
[11] P. Kurpiers, P. Magnard, T. Walter, B. Royer, M. Pechal, J. Heinsoo, Y. Salathé, A. Akin, S. Storz, J.-C. Besse *et al.*, Nature (London) **558**, 264 (2018).
[12] C. F. Ockeloen-Korppi, E. Damskägg, J.-M. Pirkkalainen, M. Asjad, A. A. Clerk, F. Massel, M. J. Woolley, and M. A. Sillanpää, Nature (London) **556**, 478 (2018).
[13] T. van Leent, M. Bock, F. Fertig, R. Garthoff, S. Eppelt, Y. Zhou, P. Malik, M. Seubert, T. Bauer, W. Rosenfeld *et al.*, Nature (London) **607**, 69 (2022).
[14] Y. Y. Gao, B. J. Lester, K. S. Chou, L. Frunzio, M. H. Devoret, L. Jiang, S. M. Girvin, and R. J. Schoelkopf, Nature (London) **566**, 509 (2019).
[15] M. Aspelmeyer, T. J. Kippenberg, and F. Marquardt, Rev. Mod. Phys. **86**, 1391 (2014).
[16] S. Barzanjeh, A. Xuereb, S. Gröblacher, M. Paternostro, C. A. Regal, E. M. Weig *et al.*, Nat. Phys. **18**, 15 (2022).
[17] T. A. Palomaki, J. D. Teufel, R. W. Simmonds, and K. W. Lehnert, Science **342**, 710 (2013).
[18] S. Barzanjeh, E. Redchenko, M. Peruzzo, M. Wulf, D. P. Lewis, G. Arnold, and J. M. Fink, Nature (London) **570**, 480 (2019).
[19] J. Chen, M. Rossi, D. Mason, and A. Schliesser, Nat. Commun. **11**, 943 (2020).
[20] S. Kotler, G. A. Peterson, E. Shojaee, F. Lecocq, K. Cicak, A. Kwiatkowski, S. Geller, S. Glancy, E. Knill, R. W. Simmonds *et al.*, Science **372**, 622 (2021).
[21] M. Mirhosseini, A. Sipahigil, M. Kalaee, and O. Painter, Nature (London) **588**, 599 (2020).
[22] M. Forsch, R. Stockill, A. Wallucks, I. Marinković, C. Gärtner, R. A. Norte, F. van Otten, A. Fiore, K. Srinivasan, and S. Gröblacher, Nat. Phys. **16**, 69 (2020).
[23] A. Wallucks, I. Marinković, B. Hensen, R. Stockill, and S. Gröblacher *et al.*, Nat. Phys. **16**, 772 (2020).
[24] I. Marinkovic, A. Wallucks, R. Riedinger, S. Hong, M. Aspelmeyer, and S. Gröblacher, Phys. Rev. Lett. **121**, 220404 (2018).
[25] N. Fiaschi, B. Hensen, A. Wallucks, R. Benevides, J. Li, T. P. Mayer Alegre, and S. Gröblacher, Nat. Photon. **15**, 817 (2021).
[26] D. Vitali, S. Gigan, A. Ferreira, H. R. Bohm, P. Tombesi, A. Guerreiro, V. Vedral, A. Zeilinger, and M. Aspelmeyer, Phys. Rev. Lett. **98**, 030405 (2007).
[27] V. Giovannetti and D. Vitali, Phys. Rev. A **63**, 023812 (2001).
[28] R. Benguria and M. Kac, Phys. Rev. Lett. **46**, 1 (1981).
[29] G. Vidal and R. F. Werner, Phys. Rev. A **65**, 032314 (2002).
[30] G. Adesso, A. Serafini, and F. Illuminati, Phys. Rev. A **70**, 022318 (2004).
[31] B. Fan, X. Lv, T. Tang, G. Deng, Y. Wang, H. Song, and Q. Zhou, OSA Continuum **4**, 2998 (2021).
[32] Q. Quan, P. B. Deotare, and M. Loncar, Appl. Phys. Lett. **96**, 203102 (2010).
[33] X. Mao, Y. Huang, K. Cui, C. Zhang, W. Zhang, and J. Peng, J. Lightwave Technol. **27**, 4049 (2009).
[34] H. Hagino, Y. Takahashi, Y. Tanaka, T. Asano, and S. Noda, Phys. Rev. B **79**, 085112 (2009).
[35] S. G. Hofer, W. Wieczorek, M. Aspelmeyer, and K. Hammerer, Phys. Rev. A **84**, 052327 (2011).
[36] D. Stefanatos, Quantum Sci. Technol. **2**, 014003 (2017).
[37] H. Miao, S. Danilishin, and Y. Chen, Phys. Rev. A **81**, 052307 (2010).
[38] C. Gut, K. Winkler, J. Hoelscher-Obermaier, S. G. Hofer, R. M. Nia, N. Walk, A. Steffens, J. Eisert, W. Wieczorek, J. A. Slater *et al.*, Phys. Rev. Res. **2**, 033244 (2020).
[39] G. Giedke, M. M. Wolf, O. Krüger, R. F. Werner, and J. I. Cirac, Phys. Rev. Lett. **91**, 107901 (2003).
[40] G. Arnold, M. Wulf, S. Barzanjeh, E. S. Redchenko, A. Rueda, W. J. Hease, F. Hassani, and J. M. Fink, Nat. Commun. **11**, 4460 (2020).
[41] C. Zhong, X. Han, and L. Jiang, Phys. Rev. Appl. **18**, 054061 (2022).
[42] C. Zhong, X. Han, H. X. Tang, and L. Jiang, Phys. Rev. A **101**, 032345 (2020).
[43] R. Riedinger, S. Hong, R. Norte, J. A. Slater, J. Shang, A. G. Krause, V. Anant, M. Aspelmeyer, and S. Gröblacher, Nature (London) **530**, 313 (2016).
[44] S. Hong, R. Riedinger, I. Marinković, A. Wallucks, S. G. Hofer, R. A. Norte, M. Aspelmeyer, S. Gröblacher, Science **358**, 203 (2017).
[45] M. J. Weaver, P. Duivestein, A. C. Bernasconi, S. Scharmer, M. Lemang, T. C. van Thiel, F. Hijazi, B. Hensen, S. Gröblacher, R. Stockill, arXiv:2210.15702.
[46] H. Sekoguchi, Y. Takahashi, T. Asano, and S. Noda, Opt. Express **22**, 916 (2014).